Self-Assembly

DOI: 10.1002/anie.201404470

Enhanced Separation of Potassium Ions by Spontaneous K^+-Induced Self-Assembly of a Novel Metal–Organic Framework and Excess Specific Cation–π Interactions**

*Wenyu Wu, Alexander M. Kirillov, Xuhuan Yan, Panpan Zhou, Weisheng Liu, and Yu Tang**

Abstract: *A novel metal–organic framework (MOF) was fabricated by spontaneous K^+-induced supramolecular self-assembly with the embedded tripodal ligand units. When the 3D ligand was loaded onto Fe_3O_4@$mSiO_2$ core-shell nanoparticles, it could effectively separate K^+ ions from a mixture of Na^+, K^+, Mg^{2+}, and Ca^{2+} ions through nanoparticle-assisted MOF crystallization into a Fe_3O_4@$mSiO_2$@MOF hybrid material. Excess potassium ions could be extracted because of the specific cation–π interaction between K^+ and the aromatic cavity of the MOF, leading to enhanced separation efficiency and suggesting a new application for MOFs.*

Metal–organic frameworks (MOFs) have been extensively applied in gas capture, catalysis, and for the development of novel chemical sensors with a high density of binding sites and superior analyte adsorption.[1] Although MOFs have been successfully used for the separation of gases, vapors, and organic molecules, their application in the separation and enrichment of metal ions remains relatively unexplored.[2] In particular, as an essential macromineral in human nutrition and the major cation inside animal cells, potassium ions are important to maintain fluid and electrolyte balance in the body,[3] thus making their selective separation and detection rather important for biomedical diagnosis and environmental remediation. To design a new method for the selective separation of potassium ions, we combined the spontaneous self-assembly of a novel MOF with a core-shell nanoparticle (Fe_3O_4@$mSiO_2$) matrix by hybridization. This method takes advantage of both the hydrophobic environment of the nanoparticle matrix and the porous structure of MOFs. The MOF units of the fabricated hybrid material have been efficiently targeted as functional components for separation. To our knowledge, this is the first example of metal-ion separation and enrichment based on a Fe_3O_4@$mSiO_2$@MOF hybrid material. The obtained hybrid material functions in aqueous media, has high selectivity, and, perhaps most importantly, is obtained by a feasible and low-cost synthetic route, thus being of both scientific and technological interest.[4]

As a result of the good hydrophilicity, biocompatibility, nontoxicity, and chemical stability,[5] core-shell magnetite materials (Fe_3O_4@$mSiO_2$) are considered as ideal materials for separation nanodevices. Although strategies to selectively isolate K^+ ions have attracted particular attention,[6] the receptor design has proven elusive, in part because the molecular architectures must be complementary to bind the K^+ target ion but rigid enough to exclude Na^+ ions. Our approach to overcome this challenge uses a flexible amide-type three-dimensional ligand L that can bind the target ion through self-assembly within the complementary cavity. This approach is similar to the host–guest interaction of metal ions within the cavity of crown ether,[7] but is less toxic and easier to synthesize. Some extraordinary examples of anion encapsulation by receptors design have been reported.[8]

As shown in Scheme 1, 4 steps are required to prepare and apply the hybrid material. The material consists of a magnetic center with good magnetic separation ability and a mesoporous silica shell with perpendicularly aligned channels (step a). The three-dimensional ligand, 1,1,1-tris{[(2′-benzylaminoformyl)phenoxy]methyl}ethane (L; Figure 1a and Scheme S1 in the Supporting Information)[9] is loaded in situ

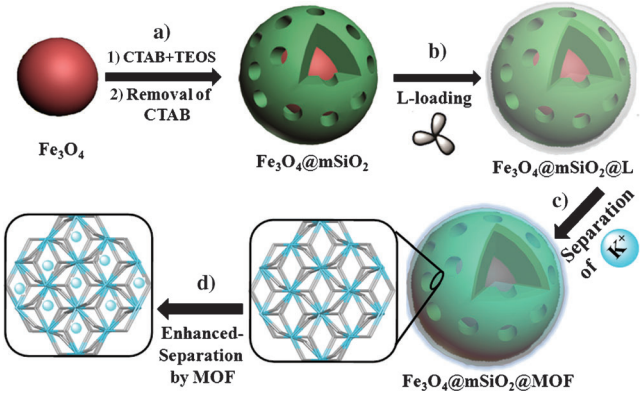

Scheme 1. Schematic representation of the fabrication and K^+ ion separation mechanism of the Fe_3O_4@$mSiO_2$@MOF hybrid material. CTAB = cetyltrimethylammonium bromide. TEOS = tetraethyl orthosilicate.

[*] W. Wu, X. Yan, P. Zhou, Prof. W. Liu, Prof. Y. Tang
Key Laboratory of Nonferrous Metal Chemistry and Resources Utilization of Gansu Province
State Key Laboratory of Applied Organic Chemistry
College of Chemistry and Chemical Engineering
Lanzhou University, Lanzhou 730000 (China)
E-mail: tangyu@lzu.edu.cn
Prof. A. M. Kirillov
Centro de Quimica Estrutural
Complexo I, Instituto Superior Tecnico
Universidade de Lisboa, Av. Rovisco Pais
Lisbon 1049-001 (Portugal)

[**] This work was financially supported by the National Natural Science Foundation of China (Project 21071068, 20931003) and the Academic Doctoral Prize (Excellent PhD Academic Awards granted by Ministry of Education) of Lanzhou University.

Supporting information for this article is available on the WWW under http://dx.doi.org/10.1002/anie.201404470.

by a direct sorption process (step b; Scheme 1). The matrix provides a hydrophobic environment for insoluble ligand L without leaching in aqueous solution, and supports the stable separation of K^+ ions by L during general environmental changes. Then, Fe_3O_4@mSiO_2@L is used for a spontaneous nanoparticle-supported K^+-induced self-assembly of the MOF from a mixture containing Na^+, K^+, Mg^{2+}, and Ca^{2+} ions (step c), and an enhanced separation occurs in the micropores of the MOF (step d). Excess K^+ ions interact with benzene rings through a specific cation–π interaction which occurs in the pores of the MOF between K^+ and the aromatic cavity, leading to enhanced separation efficiency and suggesting a new application for MOFs.

Firstly, we obtained a novel MOF through K^+-induced self-assembly of the 3D flexible amide-type L (Figure 1). X-ray crystallography shows that ligand L crystallizes with KSCN from a CH_3CN/MeOH solution (1:1 v/v) to afford single crystals. The obtained crystals are formulated as $\{[K(\mu_3\text{-}L)_2]SCN{\cdot}3\,H_2O\}_n$ (K–L),[10] in accordance with the elemental analysis and the single-crystal X-ray structure (see Tables S1 and S2 in the Supporting Information). This structure shows the formation of a 3D MOF composed of μ_3-L blocks. The compound crystallizes in a cubic space group ($Pa\bar{3}$) and the asymmetric unit contains 1 K^+ ion and one third of a molecule of L. As shown in Figure 1b, each K^+ center features a regular octahedral geometry filled by the six symmetry-equivalent O1 atoms [K–O1 2.850(3) Å] from the carbonyl groups of six tripodal ligands, whereas each ligand binds to three K^+ atoms. The crystal packing diagram reveals that flexible L blocks have a sphere-like arrangement and form cavities occupied by K^+ atoms (Figure 1c). The structure is similar to the complex of [18]crown-6 with K^+ and its derivatives, with six highly symmetrical O atoms coordinating to a central K^+ ion. The measured cavity radius of approximately 2.85 Å is comparable to those found in potassium derivatives of [18]crown-6 (2.74–2.85 Å).[11]

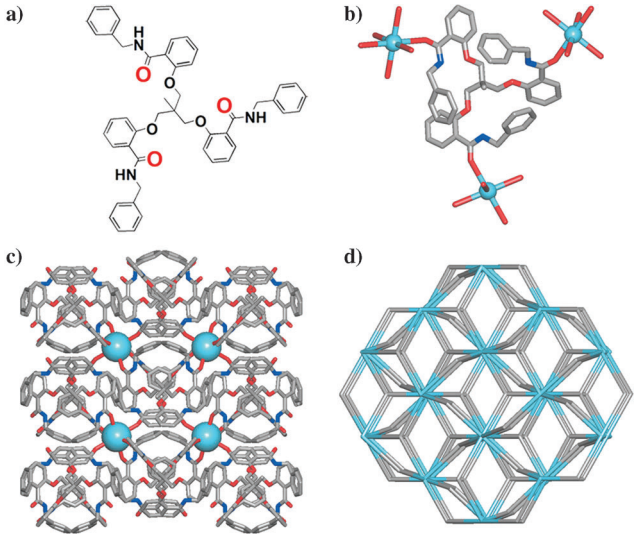

Figure 1. Crystal structure of $\{[K(\mu_3\text{-}L)_2]SCN{\cdot}3\,H_2O\}_n$ showing structural fragments. a) Chemical structure of 3D ligand L. b) μ_3 coordination mode of L and hexacoordinate $\{KO_6\}$ environment of K atoms. Atom colors: K atoms = cyan, C atoms = gray, O atoms = red, N atoms = blue. c) 3D metal–organic framework (view along the *a*-axis) with a sphere-like arrangement of L blocks generating cavities occupied by K atoms. MOF: stick model, K atoms: space-filling model. d) topological representation of the simplified binodal, 3,6-connected 3D framework with the pyrite topology. 6-connected K nodes: cyan; centroids of 3-connected μ_3-L nodes: gray.

To better understand the intricate 3D network of structure K–L, we have performed its topological analysis[12] by applying the concept of the simplified underlying net.[13] Thus, the contraction of the μ_3-L blocks to their centroids furnished an underlying net assembled from the 6-connected K^+ ions and the 3-connected μ_3-L nodes (Figure 1d). Its topological analysis shows a binodal, 3,6-connected framework with the pyrite (**pyr**) topology and the point symbol of $(6^{12}{\cdot}8^3)(6^3)_2$, wherein the $(6^{12}{\cdot}8^3)$ and (6^3) notations correspond to the K^+ and μ_3-L nodes, respectively.[14] Although a number of compounds with the **pyr** topology are reported,[12,14] this is the first alkali-metal-driven MOF of this topological type.[15]

With this result in mind, we aimed to combine the MOF material with core-shell nanoparticles to form Fe_3O_4@mSiO_2@MOF hybrid materials. By loading L into Fe_3O_4@mSiO_2 to form a nanoextractor, a nanoparticle-assisted MOF crystallization occurred after exposing the nanoextractor to K^+ ions, thus developing new applications of the MOF material and expanding its application range. A magnetization saturation value of 48.7 emu g^{-1} was measured for the Fe_3O_4@mSiO_2 nanoparticles (Figure 2a), which can quickly respond to an external magnetic field and can rapidly be redispersed homogeneously with gentle shaking (Figure 2a inset). This type of magnetic behavior enables the material to be used for simple and efficient magnetic separation of K^+ ions. FTIR spectra were used to show the ligand-loading process (Figure S1) and confirmed the formation of the L-loaded substrate. Characteristic bands are evident for ν(N–H), ν_{as}(C–H), and ν_s(C–H) at 3413, 2866, and 2929 cm^{-1}, respectively, where ν_{as} describes the asymmetric stretching mode of the bond and ν_s describes the symmetric stretch. The band for the carbonyl moiety ν(C=O) is detected at 1646 cm^{-1}, and aromatic carbon-carbon stretching vibrations are evident at 1534, 1495, and 1450 cm^{-1}, respectively, owing to the presence of L. The energy-dispersive X-ray spectrum (EDX) of the nanoextractor (Figure S2) shows the presence of nitrogen atoms that are only contained in ligand L. This result confirms the presence of L in the core-shell matrix, which is further corroborated by the thermogravimetric results (Figure S3). When the samples were heated from room temperature to 800 °C, an initial weight loss occurs for the loss of water molecules, whereas in the 483–554 °C temperature range the Fe_3O_4@mSiO_2@L loses its loaded organic block (11.86 % loss). The obtained Fe_3O_4@mSiO_2 microspheres have a uniform mesopore size (2.8 nm); the BET surface area and the total pore volume are 474.0 $m^2\,g^{-1}$ and 0.42 $cm^3\,g^{-1}$ (Figure 2b). The transmission electron microscopy (TEM) image of the resulting matrix (Figure 2c) showed that the Fe_3O_4@mSiO_2 microspheres are decorated with a compact core (approximately 90 nm in diameter) and a lower density shell of approximate thickness 20 nm (Figure 2c inset). The powder XRD patterns (Figure 2d) exhibit well-resolved diffraction peaks for Fe_3O_4@mSiO_2 and the

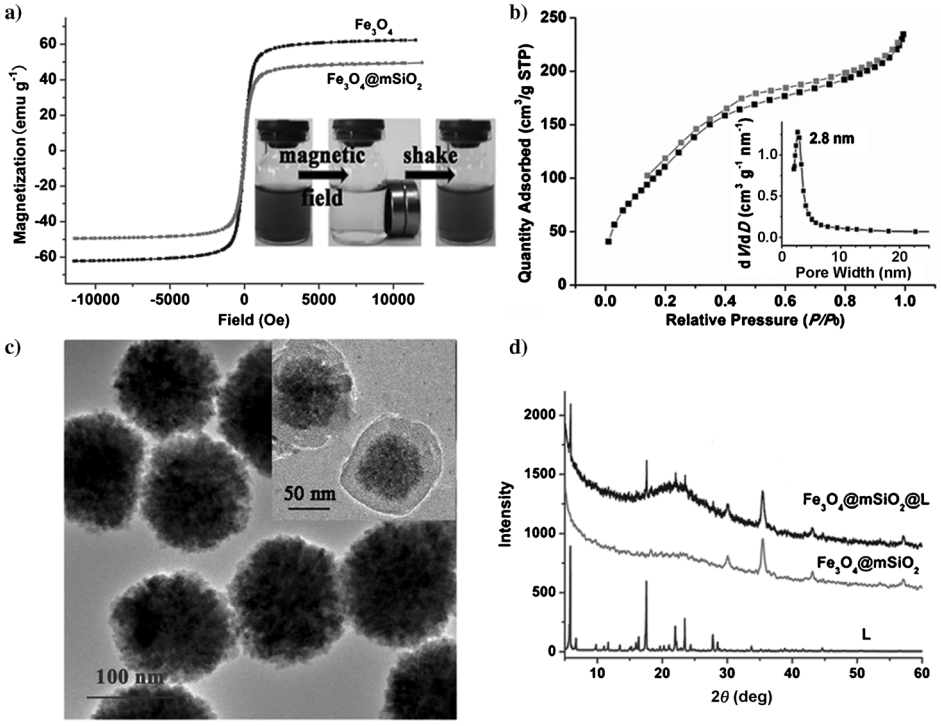

Figure 2. Characterization of Fe_3O_4, Fe_3O_4@$mSiO_2$, and Fe_3O_4@$mSiO_2$@L materials. a) Field-dependent magnetization at 300 K of Fe_3O_4 and Fe_3O_4@$mSiO_2$. Inset: Fe_3O_4@$mSiO_2$ can be separated by application of an external magnetic field and redispersed by shaking. b) N_2 adsorption/desorption isotherms for Fe_3O_4@$mSiO_2$. Inset: pore-size distribution from adsorption isotherm. V = pore volume, D = pore size. c) TEM images of the Fe_3O_4 substrate and Fe_3O_4@$mSiO_2$ microspheres (inset). d) Powder XRD patterns showing the material Fe_3O_4@$mSiO_2$ before the loading process and Fe_3O_4@$mSiO_2$@L obtained after the loading process.

nanoextractor Fe_3O_4@$mSiO_2$@L, which can be indexed to the diffraction patterns of the magnetite phase and ligand L, confirming that L has been successfully loaded.

Extraction tests were performed to evaluate the extraction efficiencies of the nanoextractor to differentiate between metal ions by saturation experiments.[16] In this method, metal ions are extracted from metal salts (which have been dissolved in water) directly by the added nanoextractor material Fe_3O_4@$mSiO_2$@L. The extent of K^+, Na^+, Ca^{2+}, or Mg^{2+} ions taken up by the nanoextractor can be indirectly determined by measuring the amount of surplus ions remaining after a simple magnetic separation. The resulting hybrid material Fe_3O_4@$mSiO_2$@MOF has a magnetization saturation value of 24.5 emu g^{-1} after the extraction of metal ions. The ability of the nanoextractor to selectively uptake K^+ ions in aqueous solution among other physiological cations was evaluated, showing excellent separation performance with extraction efficiencies of 71.7% for K^+ ions, 2.2% for Na^+, 1.4% for Ca^{2+}, and 4.9% for Mg^{2+} ions (see Table S3 in the Supporting Information). The extraction efficiency ratio for K^+ to Na^+ is almost 33-fold, where Na^+ ions are barely adsorbed by the nanoextractor in aqueous solution.[17] Interestingly, the extraction tests also showed that 3.84 equivalents of K^+ ions are extracted per 1.00 equivalent of ligand L loaded into Fe_3O_4@$mSiO_2$, subtracting the adsorption effect of matrix channels. X-ray photoelectron spectroscopy (XPS) was performed for the Fe_3O_4@$mSiO_2$@L microspheres before and after extraction of metal ions (Figure S4). The binding-energy (BE) value of the $K2p_{3/2}$ and $K2p_1$ peaks are approximately 293.1 and 296.0 eV, which were found only after the extraction experiments in aqueous solution containing both Na^+ and K^+ ions. As no significant value for Na^+ ion-binding can be detected after the extraction, it is reasonable to deduce that there is no interaction force between ligand L and Na^+. The BET surface area and the total pore volume of Fe_3O_4@$mSiO_2$@MOF also decrease to 328.1 $m^2 g^{-1}$ and 0.36 $cm^3 g^{-1}$, respectively (Figure S5), with the mesopore size slightly narrows down to 2.5 nm. These results may suggest that the effect of the channels during the separation process may be less than the surface of the matrix. Meanwhile, the powder XRD pattern shows peaks at 2θ of 19.7, 21.5, and 24.7° and can be attributed to the MOF in the Fe_3O_4@$mSiO_2$@MOF microspheres (Figure S6), suggesting that the supramolecular self-assembly of the K–L MOF and the subsequent successful metal-ion separation process occurred. Furthermore, chelating agent EDTA could strip K^+ ions from the hybrid material Fe_3O_4@$mSiO_2$@MOF (see Table S3 in the Supporting Information). Thus, the nanoextractor can be used for simple and efficient magnetic separation of K^+ ions.

Although K^+ ions form a stable MOF with ligand L, various attempts to isolate a related sodium derivative were unsuccessful, suggesting that Na^+ ions show no affinity for L. We conclude that the difference is caused by the smaller radius of Na^+, as the steric hindrance is bigger for distorting conformation between ligands during the ion-introduced self-assembly, while the ligands adopt a conformation more complementary to the coordination requirements of K^+. To further confirm the complementarity between the size of the K^+ ion and the cavity, a model containing three M (M = Na^+, K^+) ions binding to ligand L was analyzed by DFT calculations. The theoretical K–O bond length is 2.65 Å, which is close to the size of the cavity (2.85 Å), whereas the Na–O bond length (2.18 Å) is much smaller (Figure S7). Evidently, with a greater bond length to the carbonyl O atoms of ligand L, the K^+ ion can induce the self-assembly of six ligands to form an appropriate cavity which is quite similar to the cavity size of [18]crown-6. In contrast, the smaller Na^+ ion is less suitable to induce the ligands to form such a proper cavity, with a difference of 0.67 Å, thus explaining the

excellent selectivity of the L-loaded nanoextractor for K^+ ions.

To investigate in detail the extraction process involving ligand L and K^+ ions in the nanoextractor, we monitored the solution behavior of ligand L and K^+ by ^{1}H NMR spectroscopy, atomic force microscopy (AFM), and ESI-MS(+) analysis. Recording the ^{1}H NMR spectra of ligand L upon addition of increasing amounts of K^+ (from 0, 0.25, 0.5 to equimolar) showed that signals corresponding to imine ($\delta =$ 8.16 ppm) protons and adjacent methylene ($\delta = 4.51$ ppm) protons decrease and increase over time. This change is as a result of the remote shielding effect of the carbonyl O atoms, thus indicating that the reaction equilibrium is reached at the K:L molar ratio of 1:2 (Figure S8). Further addition of K^+ ions up to 1.0 equivalent led to only negligible changes. This resulted in a simplified set of signals, which we rationalized as corresponding to the $[KL_2]^+$ unit. As shown in the AFM images, the microscopic structural features of ligand L differ from its in situ formed K–L derivatives, indicating a K^+-induced agglomeration and homogenization of L (Figure 3). The presence of K^+ ions made the particles remain spherical in shape, but the average size of the particles increased (Figure 3b), as a result of the K^+-induced agglomeration of L. When extra K^+ ions was added to the agglomerated mixture of K–L, the bigger particles were interspersed with the smaller ones and tended to form nonspherical structures. The ESI-MS(+) analysis of K–L revealed an intense signal at m/z 1644.2 that also corresponds to $[KL_2]^+$ (Table S2). Therefore, we speculate that the coordination mode of the complex is uniform whether in the solid phase or in solution.

The extraction tests revealed that 3.84 equivalents of K^+ ions were extracted per 1.00 equivalent of ligand L loaded on the matrix. A fluorescence titration was carried out after adding an excess of K^+ ions to K–L, and a fluorescence-enhancement phenomenon was detected (Figure S9). Approximately 5.7% pore occupancy is populated by water-of-crystallization molecules in the MOF. Based on the DFT method calculated from the pore-size distribution diagram (Figure S10), the MOF has a typical microporous nature (pore size = 1.03 nm), suggesting that the MOF can host some excess of K^+ ions.[18] It could be surmised that the excess of K^+ ions enter the pores of the MOF and interact with benzene rings leading to a cation–π interaction,[19] which is consistent with the extraction test result. With the enhanced extraction process of the MOF platform, 3.84 equivalents of K^+ ions are extracted, a quantity which is significantly better than the stoichiometric ratio (0.50 equivalents). We reasoned that the selectivity of this substrate for surplus K^+ ions could be significantly enhanced by the cation–π interaction. More detailed studies, however, are warranted to clarify the mechanism of operation and the scope of the concept.

In conclusion, we have reported a K^+ ion-templated self-assembly with a 3D tripodal ligand L which forms a unique MOF that features a binodal, 3,6-connected net with the pyrite (**pyr**) topology. This MOF, for the first time, was identified in a coordination network driven by an alkali metal. The formation of the MOF could serve as a model for building novel and highly selective receptors for alkali-metal ions. A magnetic nanoextractor was designed to enhance the water solubility, thus allowing the application of the MOF in aqueous medium to selectively separate K^+ ions from a mixture comprising Na^+, K^+, Mg^{2+}, and Ca^{2+} ions. This separation was achieved through nanoparticle-assisted MOF crystallization by a Fe_3O_4@mSiO_2@MOF hybrid material. The spontaneous K^+-induced self-assembly of a novel MOF and its enhanced separation by a specific cation–π interaction between excess K^+ ions and the aromatic cavity of the MOF in the hybrid material may lead to a new application of MOFs to selectively detach and uptake ions, micromolecules, or biomolecules.

Received: April 19, 2014
Revised: July 14, 2014
Published online: August 11, 2014

Keywords: hybrid materials · ion extraction · metal–organic framework · potassium · self-assembly

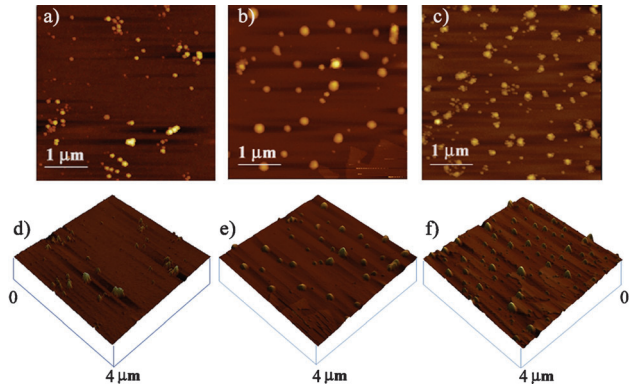

Figure 3. AFM images illustrating the binding of K^+ to ligand L to form particles. a), d) Ligand L agglomerates with average size 80 ± 10 nm. b), e) Particles of [L + K^+] with increased average size 150 ± 40 nm. c), f) Particles formed from ligand L and K^+ (5 equiv) [L + 5 K^+] with average spherical particle size 100 ± 30 nm. The angled view of the AFM images is shown in (d)–(f).

[1] a) J. R. Li, Y. Ma, M. C. McCarthy, J. Sculley, J. Yu, H. K. Jeong, P. B. Balbuena, H. C. Zhou, *Coord. Chem. Rev.* **2011**, *255*, 1791 – 1823; b) N. B. Shustova, A. F. Cozzolino, S. Reineke, M. Baldo, M. Dincă, *J. Am. Chem. Soc.* **2013**, *135*, 13326 – 13329; c) J. Lee, O. K. Farha, J. Roberts, K. A. Scheidt, S. T. Nguyen, J. T. Hupp, *Chem. Soc. Rev.* **2009**, *38*, 1450 – 1459; d) L. E. Kreno, K. Leong, O. K. Farha, M. Allendorf, R. P. Van Duyne, J. T. Hupp, *Chem. Rev.* **2012**, *112*, 1105 – 1125.

[2] a) J. R. Li, R. J. Kuppler, H. C. Zhou, *Chem. Soc. Rev.* **2009**, *38*, 1477 – 1504; b) J. R. Li, J. Sculley, H. C. Zhou, *Chem. Rev.* **2012**, *112*, 869 – 932.

[3] "Potassium Ion Channels: Molecular Structure, Function, and Diseases": *Current Topics in Membranes, Vol. 46* (Eds.: Y. Kurachi, L. Y. Jan, M. Lazdunski), Academic Press, San Diego, CA, **1999**.

[4] a) N. Schüwer, H.-A. Klok, *Adv. Mater.* **2010**, *22*, 3251 – 3255; b) Z. Liu, F. Luo, X. J. Ju, R. Xie, T. Luo, Y. M. Sun, L. Y. Chu, *Adv. Funct. Mater.* **2012**, *22*, 4742 – 4750; c) S. Y. Lin, S. W. Liu, C. M. Lin, C. H. Chen, *Anal. Chem.* **2002**, *74*, 330 – 335; d) R. A. Maurya, C. P. Park, J. H. Lee, D.-P. Kim, *Angew. Chem.* **2011**, *123*, 6074 – 6077; *Angew. Chem. Int. Ed.* **2011**, *50*, 5952 – 5955.

[5] a) M. F. Shao, F. Y. Ning, J. W. Zhao, M. Wei, D. G. Evans, X. Duan, *J. Am. Chem. Soc.* **2012**, *134*, 1071 – 1077; b) S. S. Liu, H. M. Chen, X. H. Lu, C. H. Deng, X. M. Zhang, P. Y. Yang, *Angew. Chem.* **2010**, *122*, 7719 – 7723; *Angew. Chem. Int. Ed.* **2010**, *49*, 7557 – 7561; c) A. K. Gupta, M. Gupta, *Biomaterials* **2005**, *26*, 3995 – 4021; d) M. J. Lü, J. Li, X. Y. Yang, C. A. Zhang, J. Yang, H. Hu, X. B. Wang, *Chin. Sci. Bull.* **2013**, *58*, 2698 – 2710.

[6] M. E. Davis, *Nature* **2002**, *417*, 813 – 821.

[7] a) G. W. Gokel, W. M. Leevy, M. E. Weber, *Chem. Rev.* **2004**, *104*, 2723 – 2750; b) X. F. Zhou, F. Y. Su, Y. Q. Tian, C. Youngbull, R. H. Johnson, D. R. Meldrum, *J. Am. Chem. Soc.* **2011**, *133*, 18530 – 18533; c) W. L. Wei, C. Xu, J. S. Ren, B. L. Xua, X. G. Qu, *Chem. Commun.* **2012**, *48*, 1284 – 1286.

[8] a) R. Custelcean, P. Remy, P. V. Bonnesen, D. E. Jiang, B. A. Moyer, *Angew. Chem.* **2008**, *120*, 1892 – 1896; *Angew. Chem. Int. Ed.* **2008**, *47*, 1866 – 1870; b) R. Custelcean, A. Bock, B. A. Moyer, *J. Am. Chem. Soc.* **2010**, *132*, 7177 – 7185; c) C. D. Jia, B. Wu, S. G. Li, X. J. Huang, Q. L. Zhao, Q. S. Li, X. J. Yang, *Angew. Chem.* **2011**, *123*, 506 – 510; *Angew. Chem. Int. Ed.* **2011**, *50*, 486 – 490.

[9] X. H. Yan, Z. H. Cai, C. L. Yi, W. S. Liu, M. Y. Tan, Y. Tang, *Inorg. Chem.* **2011**, *50*, 2346 – 2353.

[10] Crystal data for (K – L): $[C_{95}H_{90}KN_7O_{12}S]$; $M_r = 1592.90$; cubic; space group $Pa\bar{3}$; $a = 20.4860(14)$, $b = 20.4860(14)$, $c = 20.4860(14)$ Å; $V = 8597.5(10)$ Å^3; $D_{calcd} = 1.231\ g\,cm^{-3}$; μ(Mo $K\alpha$) $= 0.152\ mm^{-1}$; $T = 296(2)$ K; 58818 independent reflections measured; F^2 refinement; $R_1 = 0.0956$; $wR_2 = 0.2324$. CCDC 998191 contains the supplementary crystallographic data for this paper. These data can be obtained free of charge from The Cambridge Crystallographic Data Centre via www.ccdc.cam.ac.uk/data_request/cif.

[11] J. W. Steed, *Coord. Chem. Rev.* **2001**, *215*, 171 – 221.

[12] V. A. Blatov, *IUCr CompComm Newsletter* **2006**, *7*, 4 – 38.

[13] a) V. A. Blatov, D. M. Proserpio in *Modern Methods of Crystal Structure Prediction* (Ed.: A. R. Oganov), Wiley, Hoboken, **2010**, pp. 1 – 28; b) V. A. Blatov, M. O'Keeffe, D. M. Proserpio, *CrystEngComm* **2010**, *12*, 44 – 48; c) E. V. Alexandrov, V. A. Blatov, A. V. Kochetkova, D. M. Proserpio, *CrystEngComm* **2011**, *13*, 3947 – 3958; d) M. O'Keeffe, O. M. Yaghi, *Chem. Rev.* **2012**, *112*, 675 – 702.

[14] a) M. O'Keeffe, M. A. Peskov, S. J. Ramsden, O. M. Yaghi, *Acc. Chem. Res.* **2008**, *41*, 1782 – 1789; b) H. K. Chae, J. Kim, O. D. Friedrichs, M. O'Keeffe, O. M. Yaghi, *Angew. Chem.* **2003**, *115*, 4037 – 4039; *Angew. Chem. Int. Ed.* **2003**, *42*, 3907 – 3909.

[15] a) R. D. Shannon, *Acta Crystallogr. Sect. A* **1976**, *32*, 751 – 767; b) C. Lee, W. Yang, R. G. Parr, *Phys. Rev. B* **1988**, *37*, 785 – 789; c) A. D. Becke, *J. Chem. Phys.* **1993**, *98*, 5648 – 5652; d) F. H. Allen, *Acta Crystallogr. Sect. B* **2002**, *58*, 380 – 388.

[16] a) M. Liu, A. Bertova, N. Illy, B. Brissault, J. Penelle, K. Ondriasb, V. Barbier, *RSC Adv.* **2012**, *2*, 8606 – 8609; b) S. Kopolow, T. E. Hogen Esch, J. Smid, *Macromolecules* **1973**, *6*, 133 – 142.

[17] A. Thibon, V. C. Pierre, *J. Am. Chem. Soc.* **2009**, *131*, 434 – 435.

[18] Y. J. Cui, Y. F. Yue, G. D. Qian, B. L. Chen, *Chem. Rev.* **2012**, *112*, 1126 – 1162.

[19] G. W. Gokel, L. J. Barbour, R. Ferdani, J. X. Hu, *Acc. Chem. Res.* **2002**, *35*, 878 – 886.

